Solar Energy 245 (2022) 158–164

Contents lists available at ScienceDirect

Solar Energy

journal homepage: www.elsevier.com/locate/solener

Orthogonal modulation based light beam induced current method for anti-noise defect detection in photovoltaic cells

Dongwen Gan [a], Lei Quan [a,*], Fan Zhu [a], Kai Xie [a], Junmei Bai [b]

[a] School of Aerospace Science and Technology, Xidian University, Xi'an, Shaanxi, 710126, China
[b] Xi'an Fenghuo Electronic Technology Co., Ltd, Xi'an, Shaanxi, 710075, China

ARTICLE INFO

Keywords:
Defect detection
Orthogonal modulation
Light beam induced current
Noise immunity
Photovoltaic cells

ABSTRACT

In this paper, orthogonal modulation theory is introduced into light beam-induced current (LBIC) scanning to develop an orthogonal modulation-based LBIC (OMLBIC) method that is proposed for anti-noise defect detection applications in photovoltaic cells. In the proposed method, the response signal from the scanning area is treated similarly to the characteristics of a communication channel; first, orthogonal structured light patterns are generated to illuminate the scanning area surface, the combined current output of the entire device is then measured for each pattern, and demodulation is finally performed to extract the signal precisely from the noise. The feasibility of the proposed method and its detection performance were evaluated. The experimental results indicate that the proposed method can cause a maximum mean square error (MSE) reduction of 16,384 times with 128 × 128 scanning points, and it provides an enhanced direct link between the inherent spatial non-uniformities and the overall current map for the sample. When compared with the conventional LBIC method, the OMLBIC method provided increased consistency during noisy scanning, greater detail in defect detection, and a reduction in the sensitivity to noise, without requiring any time-consuming increase in sampling or hardware upgrades. The association between the noise elimination effect and the size of the structured light pattern was also studied to provide a superior system configuration. The proposed method shows major potential for improvement in the defect detection accuracy and classification of photovoltaic cells in industrial applications.

1. Introduction

Industrial solar cells are composed of large-area junctions(Kaminski et al., 2003) that can contain various defects, including broken gates, wafer cracking, fragmentation, breakage, electrode breakdown, scratches, or dirty cells(Chen et al., 2020; Fuyuki et al., 2005). The defective area then cannot generate a current, which seriously affects the cell's conversion efficiency(Lim et al., 2015; Su et al., 2022). A comprehensive, precise, practical, and nondestructive defect detection method can provide a valuable current map that will help to improve the fabrication technology, aid in the production of efficient and reproducible solar cells(Carstensen et al., 2003), and thus increase the industrial mass production yield(Wang et al., 2021).

Several approaches to locating defects in solar cells have been studied. The electron beam-induced current (EBIC) method measures the variations in the solar cell current caused by the electron beam of a scanning electron microscope (SEM) and achieves high spatial resolution(Zhao et al., 2021). However, the size of the microscope's lens limits the scanning area, and the high vacuum atmosphere required for EBIC greatly restricts its industrial application(Kittler et al., 2002; Reuter et al., 2011). The electroluminescence (EL) method adds a bias voltage between the photovoltaic materials and then images the weak infrared radiation generated by the EL of the photovoltaic materials, which provides results rapidly(Demirci et al., 2021). However, the EL image contains a mixture of information about the wafer structure layout and the actual defects, and the weak emitted light only contains the wavelengths from within a small spectral range and thus cannot represent the actual defects or the photoelectric conversion efficiency for the entire spectrum(Fuyuki and Kitiyanan, 2009). Both the EBIC and EL methods acquire current maps in an equivalent manner and thus cannot provide a complete representation of the practical operating status of the solar cells under test.

The light beam-induced current (LBIC) method, a comparatively basic but highly effective, nondestructive, and noncontact diagnostic

* Corresponding author at: No. 266 Xinglong Section of Xi Feng Rd., Xi'an, Shaanxi, 710126, China.
E-mail addresses: dwgan@stu.xidian.edu.cn (D. Gan), quanlei@xidian.edu.cn (L. Quan), fanzhu@stu.xidian.edu.cn (F. Zhu), kaixie@mail.xidian.edu.cn (K. Xie), baijm1988@163.com (J. Bai).

https://doi.org/10.1016/j.solener.2022.08.058
Received 23 May 2022; Received in revised form 3 August 2022; Accepted 21 August 2022

tool, can provide comprehensive, effective, and practical assessments via direct detection of both structural and process-induced defects(Lim et al., 2015; Vorasayan et al., 2009). The LBIC system focuses the beam from an isolated light source onto the cell to produce a photogenerated current, and the short-circuit current can be acquired immediately when using this method, thus providing a direct link between the inherent spatial nonuniformities and the overall performance of the cells(Lim et al., 2015; Sites and Nagle, 2005). Additionally, the configurable parameters of LBIC systems, which include the wavelength, the voltage bias, and the light intensity, enable a comprehensive assessment of the performance of photovoltaic cells(Geisthardt and Sites, 2014b; Orlov et al., 2014). However, in the conventional LBIC method, movement of the sample across a fixed laser beam using controlled stepper motors (Geisthardt and Sites, 2014a; Kaminski et al., 2003) or shifting the beam across a fixed sample(Acciarri et al., 2002; Carstensen et al., 2003) will lead to weakness in the system's positioning accuracy and will also introduce mechanical vibration noise. Additionally, the inefficiency of the mechanical movement and the single-point scanning mode both greatly limit the defect detection speed(Geisthardt and Sites, 2014b; Koktavy et al., 2007).

The introduction of structured light provides a nonmechanical scanning method for LBIC. The use of the multi-laser LBIC method(Bliss et al., 2016; Jeco et al., 2016; Vorasayan et al., 2009) provides an improvement in either speed or accuracy when compared with the conventional LBIC method, and the compressive sensing-based LBIC method reduces the measurement time(Hall et al., 2016; Koutsourakis et al., 2016; Koutsourakis et al., 2015; Quan et al., 2019; Quan et al., 2017). These methods thus increase the detection speed with a small degree of performance deterioration when compared with the conventional LBIC method(Kumar et al., 2021).

In the conventional LBIC method, the main factor that currently restricts improvements in measurement precision is the scanning method's sensitivity to noise. The sensitivity of LBIC systems is largely determined by two factors. On the one hand, a photovoltaic cell is a large-area p-n junction, and its output represents the combination of the short-circuit currents induced over the entire illuminated area of the cell(Azim, 2013). The noise current that is introduced is caused by thermal noise from the amplifier(Motchenbacher and Connelly, 1993), power supply-induced jitter(Tripathi et al., 2019), leakage from the light source, halos caused by lens distortion, and the dark current(Pulfrey, 1978) of the solar cell itself, which may be so high that it distorts the light beams induced current signal. Among these factors, the output noise from the entire solar cell mainly comes from the light source jitter and the leakage and interference coming from the adjacent test point. The light source jitter is mainly affected by the power supply used for the light source device. However, light leakage from the illuminated test point also contributes to the noise at the adjacent dark test point. Since the light source jitter and the light leakage are often Gaussian, zero-mean and independent, the noise caused by these factors is often zero-mean Gaussian noise. In other words, the output signal from the scanning process is mainly disturbed by uncorrelated zero-mean Gaussian noise.

Inspired by modulation theory, these detection procedures can be regarded as modulation processes in a Gaussian channel. The noise-sensitive signal can be coded into a modulated-type signal, and with an appropriate demodulation method, the useful signal can be extracted accurately and efficiently from the noise-corrupted modulated signal.

In this study, an orthogonal modulation-based LBIC (OMLBIC) method is proposed for anti-noise defect detection in photovoltaic cells. This method uses orthogonal modulation to eliminate the noise interference and extracts the current map from the modulated signal. We choose Hadamard multiplexing to design the orthogonal modulation system, which provides a considerable reduction in the mean square error (MSE) of the recovered current map in the presence of additive random noise(Podlaskin, 2007; Streeter et al., 2009). During the modulation procedure, the orthogonal modulated structured light is focused on the surfaces of the solar cells, and the photocurrent induced by the entire testing area is obtained as a single measurement value. During the demodulation procedure, the current map is extracted from the noise-submerged modulated signal by an inverse Hadamard matrix multiplexing process. The primitive noise is compressed and the non-correlated part of the signal is eliminated. The OMLBIC method proposed here represents an anti-noise detection algorithm that provides a current map with a lower MSE than the conventional LBIC method without any additional detection time consumption or hardware upgrade requirements.

The rest of this paper is organized as follows. In Section 2, the system for the proposed OMLBIC method is briefly introduced. The experimental results and their analysis are presented in Section 3. The discussion of these results is then presented in section 4. Finally, Section 5 presents conclusions about the work.

2. System model

Unlike the conventional LBIC system, the proposed method uses pattern-controlled structured light to illuminate multiple points in the testing area, in which the control patterns were designed carefully to ensure the orthogonality of each projection. Then, each pattern corresponds to the current response of the testing area, i.e., the combination of the outputs from all illuminated test points is amplified and measured. Finally, a more precise current map of the entire measurement area can be recovered using a demodulation algorithm and the defect locations can be observed clearly.

A schematic of the measurement setup used is shown in Fig. 1. An industrial computer-controlled projector is used as the structured light source and controls the brightness, pattern, and speed of the structured light. The light beams emitted by the projector are then received by the solar cells. The total photoelectric current induced in the sample cell is collected using a transimpedance amplifier, and is then sampled and quantized using an analog-to-digital converter (ADC). The control computer is used to generate orthogonal pattern signals for the projector and also to apply the demodulation algorithm to reconstruct the current map of the sample under test.

The scanning procedure is shown in Fig. 2 from the perspectives of both modulation and demodulation. The signal from the sample cell is modulated using a series of orthogonal pattern-controlled structured light beams, and the additive noise signal is compressed by the modulation process simultaneously. Note that each structured light beams consists of a column of the orthogonal matrix, and that the value of the modulated signal is generated in each scanning period. The combination of the modulated signal and the compressed noise is then obtained as the measurements. Finally, the signal with the residual noise content is extracted as the final output via the demodulation process. Following the modulation and demodulation processes, the noise level decreased for the following reasons. First, the noise introduced by the light beams has a zero-mean Gaussian distribution. Second, each of the noise signals introduced by the sampling process is uncorrelated to the other noise signals.

In fact, the anti-noise performance of the proposed method can be estimated exactly using modulation theory, and is derived as follows. In a solar cell, the current map of the testing area is represented by a two-dimensional image $\boldsymbol{X}$ composed of n rows and n columns, which can be vectored vertically to form an n^2-dimensional vector $\boldsymbol{v}$ as follows:

$$v_k = x_{i,j}, \{i \in [1,n]; j \in [1,n]; k = (i-1)n + j\} \tag{1}$$

where v_k is the kth element of the signal vector $\boldsymbol{v}$, and $x_{i,j}$ represents the ith row and the jth column of the current map.

When Hadamard encoding is used as the modulation scheme, the modulation procedure with random additive noise can be simplified as shown in Fig. 3. The Hadamard H-matrix of order n^2(Harwit and Sloane, 1979a), which is denoted by $\boldsymbol{H}$, is used as the measurement matrix. The elements of $\boldsymbol{H}$ control the brightness of the structured light beams,

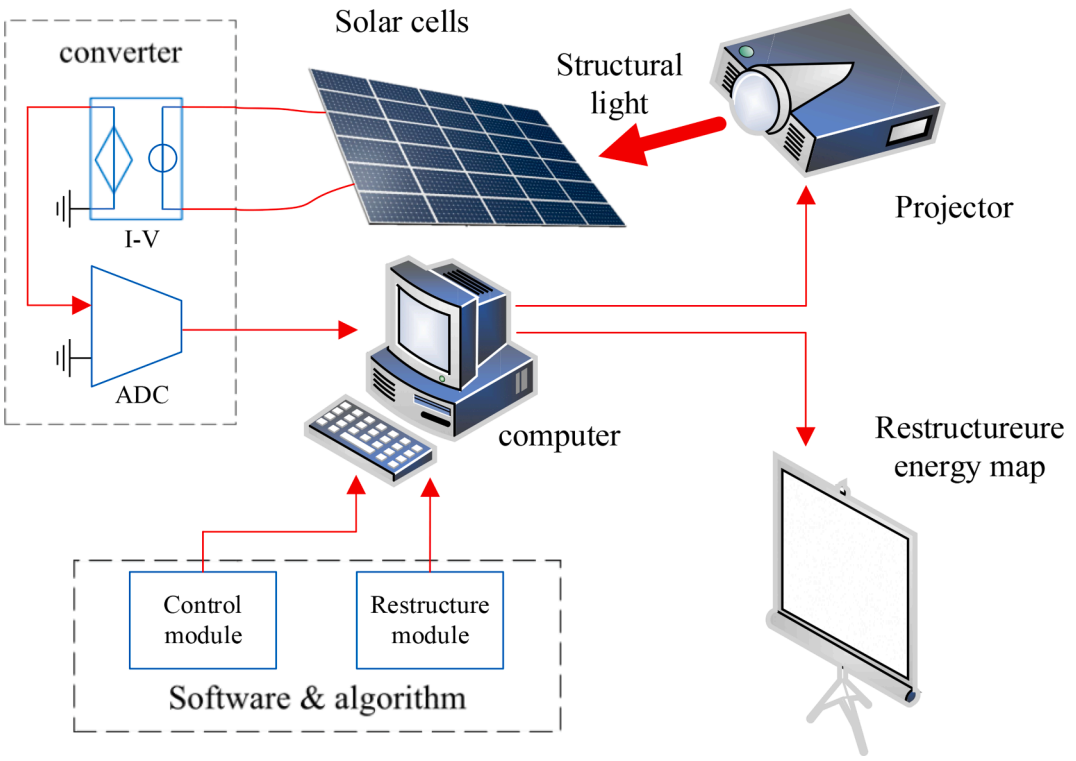

Fig. 1. System structure used for the OMLBIC method.

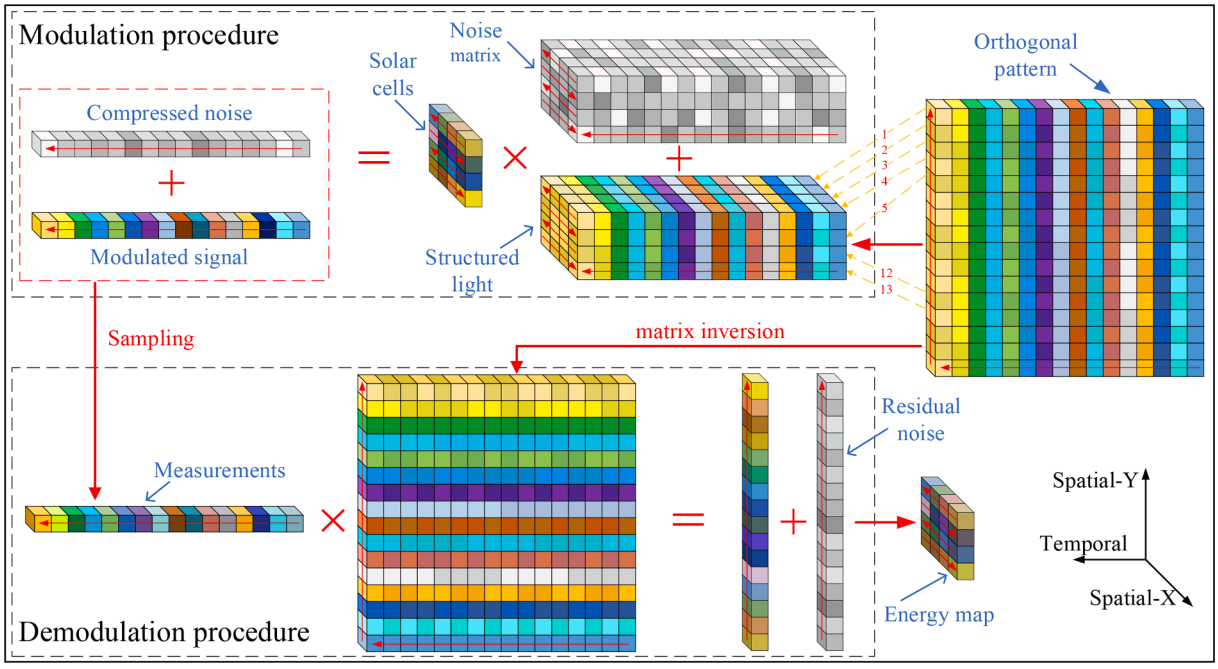

Fig. 2. Schematic diagram of the signal path for the OMLBIC method.

where elements with a value of 1 correspond to bright beams and elements with a value of −1 correspond to dark beams.

Note here that the induced current shows a linear response to the intensity of the incident light beams. Each illumination period generates an entire current output composed of the current induced by the light beams and the spatial noise-induced current. The spatial noise matrix signal can be compressed into the additive temporal noise vector signal $\boldsymbol{e} \in R^{n^2}$. The measurement procedure can then be expressed as:

$$y_i = h_i \boldsymbol{v} + e_i = \sum_{j=1}^{n^2} h_{i,j} v_j + \sum_{j=1}^{n^2} e_{i,j}, i \in \left[1, n^2\right] \tag{2}$$

where y_i is the ith element of the observation vector $\boldsymbol{y} \in R^{n^2}$, and h_i represents the ith row of the Hadamard matrix $\boldsymbol{H}$.

The complete modulation procedure for the OMLBIC method can be modeled as:

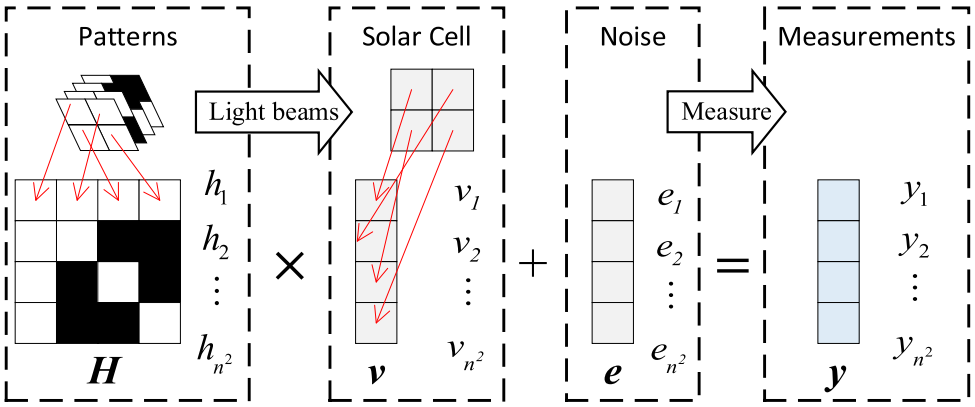

Fig. 3. Simplified modulation procedure for the OMLBIC system with 4 × 4 test points.

$$\boldsymbol{y} = \boldsymbol{H} \times \boldsymbol{v} + \boldsymbol{e} \tag{3}$$

After n measurements are collected to form a vector $\boldsymbol{y}$, the entire current map of the solar cells can be reconstructed by applying the demodulation procedure:

$$\boldsymbol{v}_{OMLBIC} = \boldsymbol{H}^{-1} \times \boldsymbol{y} = \boldsymbol{v} + \boldsymbol{H}^{-1} \times \boldsymbol{e} \tag{4}$$

where $\boldsymbol{v}_{OMLBIC}$ is the reconstructed current signal for the OMLBIC method, and $\boldsymbol{H}^{-1} \times \boldsymbol{e}$ is the residual noise of this reconstructed current signal.

The MSE is used as the evaluating indicator and can be expressed as:

$$MSE(\boldsymbol{f}, \boldsymbol{g}) = \frac{1}{MN} \sum_{i=1}^{M} \sum_{j=1}^{N} \left(f_{ij} - g_{ij}\right)^2 \tag{5}$$

where $\boldsymbol{f}$ and $\boldsymbol{g}$ represent the reference signal and the test signal, respectively, which both are of the size $M \times N$.

For the proposed OMLBIC system with its so-called Hadamard advantage(Harwit and Sloane, 1979b; Streeter et al., 2009), the MSE is.

$$MSE(\boldsymbol{v}, \boldsymbol{v}_{OMLBIC}) = \left\|\boldsymbol{H}^{-1} \times \boldsymbol{e}\right\|_2^2 / n^2 = \sigma_0^2 / n^2 \tag{6}$$

where $\|\|_2$ represents the L_2-norm, and σ_0^2 is the noise variance of the OMLBIC system.

In terms of the LBIC system, the modulation and demodulation procedure can be modeled as follows:

$$\begin{aligned} \hat{\boldsymbol{y}} &= \boldsymbol{I} \times \boldsymbol{v} + \hat{\boldsymbol{e}} \\ \boldsymbol{v}_{LBIC} &= \boldsymbol{I}^{-1} \times \hat{\boldsymbol{y}} = \boldsymbol{v} + \hat{\boldsymbol{e}} \end{aligned} \tag{7}$$

where $\boldsymbol{I}$ is the measurement matrix, $\hat{y}$ is the observation vector, $\boldsymbol{v}_{LBIC}$ is the reconstructed current signal, and $\hat{e}$ is the residual noise. The MSE of the reconstructed current map in the LBIC system is then given by:

$$MSE(\boldsymbol{v}, \boldsymbol{v}_{LBIC}) = \|\hat{\boldsymbol{e}}\|_2^2 / n^2 = \sigma_1^2 \tag{8}$$

where σ_1^2 is the noise variance of the LBIC system.

Therefore, when compared with LBIC, the proposed OMLBIC method obtains a gain of:

$$\frac{MSE(\boldsymbol{v}, \boldsymbol{v}_{LBIC})}{MSE(\boldsymbol{v}, \boldsymbol{v}_{OMLBIC})} = \left(n \cdot \frac{\sigma_1}{\sigma_0}\right)^2 \tag{9}$$

which indicates that an increase in the number of test points n or a reduction in the noise variance σ_0 would result in significant performance improvement in the proposed OMLBIC method.

In terms of area scanning of M row pixels and N column pixels, because the rank of the Hadamard matrix can only be a power of two, thus the order of the Hadamard matrix.

$$n^2 = 2^{\lceil \log_2(M \times N) \rceil} \tag{10}$$

where $\lceil\rceil$ is the ceiling function. It is possible to enlarge the signal dimension to a power of two by tail zeroing without destroying the orthogonality of the modulation procedure. Therefore, the OMLBIC method can be applied to area scanning of arbitrary points.

3. Experiments

In this section, the scanning performance of the proposed OMLBIC method is evaluated using a section of an industrial solar cell and various types of simulated defects. Then, the performance of the OMLBIC method is studied when using different system configurations. Additionally, the results for the conventional LBIC method were generated using the same device and configurations to act as a benchmark for comparison.

3.1. Configurations

A practical implementation of the system shown schematically in Fig. 1 was constructed. A digital industrial projector with a monochromatic red light with an operating wavelength of 650 nm, a power intensity of 0.49 W, and a pixel width of 100 μm was used as the pixel light source. An approximately 15 × 12 mm^2 sample was cut from a standard polycrystalline silicon solar cell for use as the sample cell, and the typical defect types were simulated by pasting translucent paper samples of various shapes onto the surfaces of the sample solar cells, as illustrated in Fig. 4. The scanning area was set to 128 × 128 to cover the various defects in the solar cell. The current induced in the sample was amplified using a transimpedance amplifier and sampled using a 24-bit ADC. A control computer was used to acquire these measurements and then recover the current map of the scanning area using the reconstruction algorithm, which was implemented using MATLAB(R2020b, 2020). In addition, the Hadamard matrix-based pattern generation and control processes for the structured light were also performed using the control computer. Finally, all experiments were conducted in a dark room to obtain the best possible results.

3.2. Results and analysis

First, an experiment using the proposed OMLBIC method with 128 × 128 test points and a pixel width of 100 μm was conducted, and the recovered current map is shown in Fig. 5.

The figure clearly shows that the OMLBIC method could obtain the exact current map of the sample cell. Defects such as the edge, finger, and welding area defects in the sample cell were shown clearly, and the variations in the photoelectric efficiency, which were caused by the pasting of the translucent paper, were reflected faithfully on the current

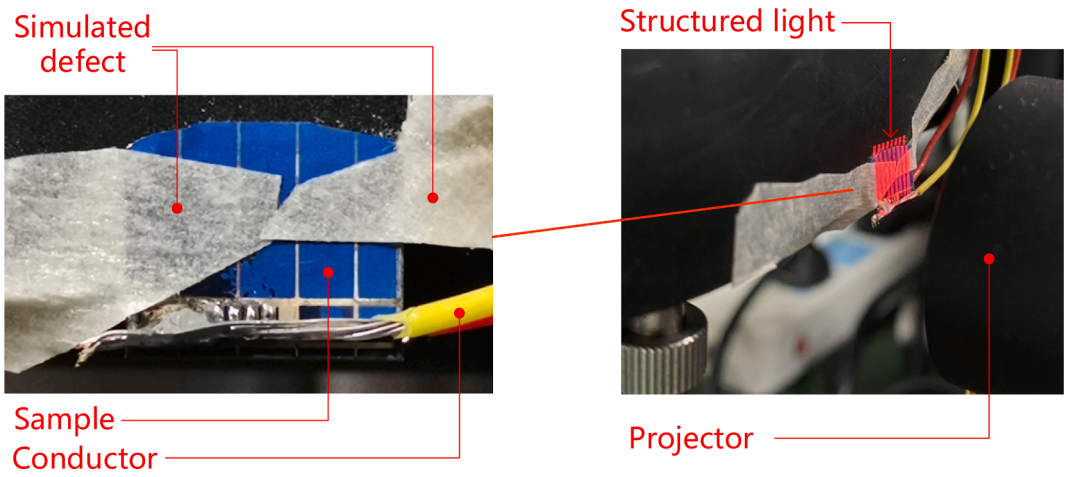

Fig. 4. Practical implementation of the OMLBIC system.

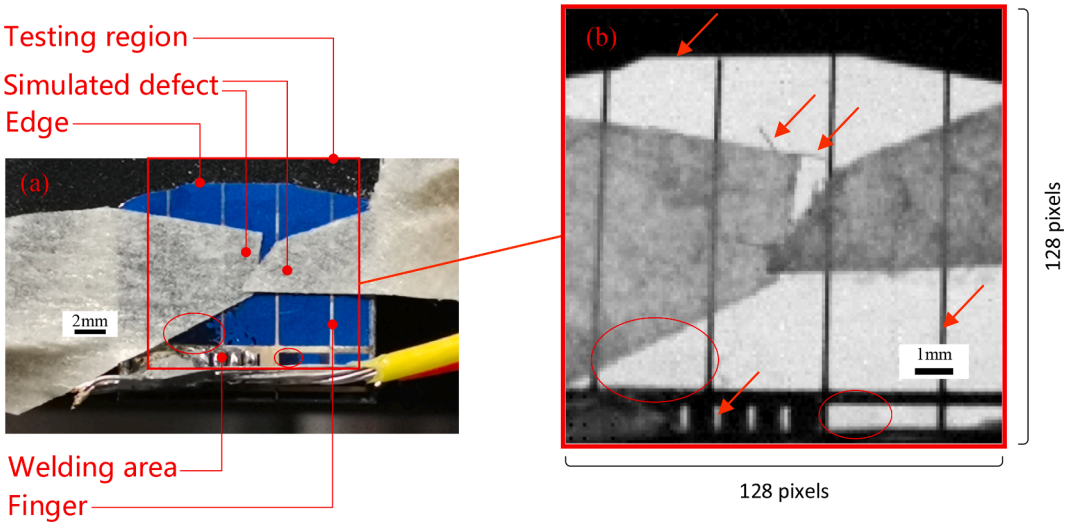

Fig. 5. (a) Various defects in the sample cells and (b) the defects located in the current map.

map. Additionally, invisible defects that can hardly be recognized in the optical image, were located correctly. In particular, it was shown that the dirty area on the optical image had little effect on the photoelectric efficiency and thus should not be judged to be a defect.

Second, experiments using the proposed OMLBIC method with 32 × 32, 64 × 64, and 128 × 128 test points and a resolution of 100 μm were conducted. The results obtained with the conventional LBIC method when using the same configurations were also generated for comparison. The normalized current maps of the sample solar cell produced by these two methods are shown in Fig. 6.

These maps show that both LBIC and OMLBIC could recover current maps of the sample cell. However, the current map obtained using LBIC suffers from heavy noise corruption, including noticeable Gaussian noise and stripe noise, while that acquired using OMLBIC suffers only light Gaussian noise and no stripe noise. Additionally, when the number of sampling points was increased, the quality of the current map improved significantly for the OMLBIC method, while little improvement was shown in the maps generated by LBIC.

These results indicate that the zero-mean additive noise could be eliminated well by the modulation process, and that the noise suppression effect increases rapidly in tandem with increases in the number of test points used. Specifically, at the resolution of 32 × 32, OMLBIC was able to recover the finger image of the sample cell clearly, while that obtained using LBIC is difficult to distinguish. Furthermore, at the resolution of 64 × 64, detailed characteristics of defects such as the invisible defect and the shape of the transparent paper can be seen clearly in the current map of OMLBIC, while the shape and the edge of the defect are difficult to recognize in the LBIC map. Finally, at the resolution of 128 × 128, the current map from OMLBIC showed more detail, including the welding area, the edges of the sample cells, and the transparency of the translucent paper, while that from LBIC suffers heavily from stripe noise, thus making it difficult to distinguish between stripe noise and small defects. Note that the stripe noise was only present in the results from LBIC; this noise may be caused by instability of the amplifier, the ADC, or the power supply, and it has a considerable effect on serial point-by-point scanning. In the experiment, a negligible number of calibration frames is inserted to provide a relative output correction, and differential measurement voltage is obtained as the actual output of the solar cells, in order to eliminate the drift of the amplifier. The OMLBIC method explores both the spatial and temporal correlations of the signal by performing modulation and demodulation using structured light beams. Therefore, the signal jitter caused by the instabilities was averaged and dispersed over the entire scanning area, which essentially eliminated the stripe noise.

4. Discussion

In general, the OMLBIC method obtained clearer current maps than

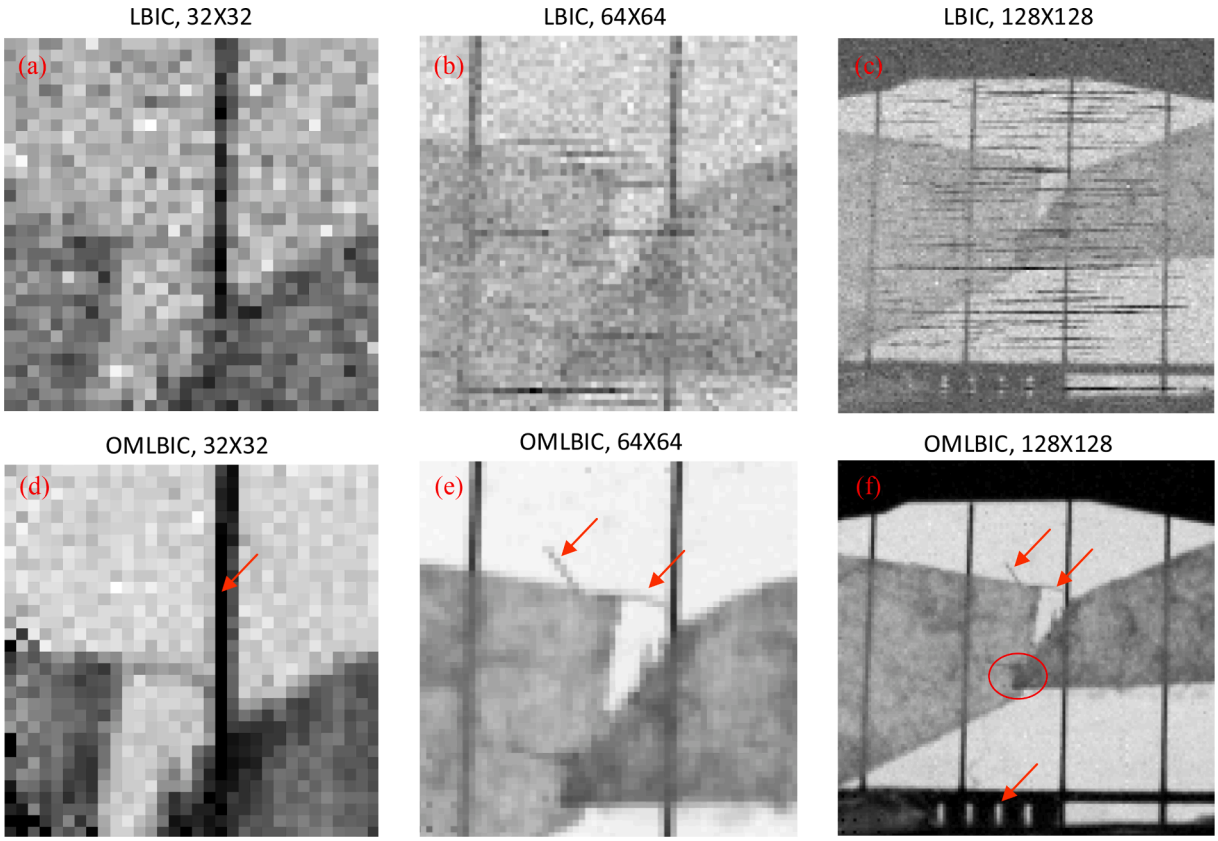

Fig. 6. Effect comparison between the OMLBIC method and the LBIC method.

the conventional LBIC method when using the same hardware configurations. Theoretically, when compared with LBIC, the OMLBIC method can achieve a maximum MSE ratio gain of $M \times N$ at a current map of M row pixels and N column pixels. However, the performance gain of the OMLBIC method is mainly limited by two factors. On the one hand, the spatial resolution and the accuracy of the current signal that can be obtained are determined for several reasons. Firstly, the dynamic range of the amplifier limits the maximum value of the signal; Secondly, the precision of the ADC restricts the recognizable minimum variation of the signal; At last, the drift and power supply rejection ratio limits the noise level of the analog devices. On the other hand, an increase in the number of light beams will bring increased adjacent light interference, which will then limit the increase in the gain of the OMLBIC method. The gain of the OMLBIC method can also be improved by reducing the overall noise level of the OMLBIC system. However, the noise level is determined by the light leakage from the projector and the ambient light, and thus can be improved further by upgrading the projector and reducing the ambient light.

5. Conclusion

In this study, by a process of introducing orthogonal modulation into the LBIC method, we have developed a noncontact, noise-insensitive, high-precision, and multi-spot scanning method for defect detection in photovoltaic cells. The proposed method introduced an orthogonal modulation-based multi-spot scanning method to explore the correlations of the signal with the zero-mean and independent characteristics of the noise, thus resulting in a much higher anti-noise performance and much higher scanning accuracy. A theoretical analysis of the modulation and demodulation processes was performed to guarantee the uncorrelated noise elimination performance and the decoupling of the current map signal of the scanning area. The experimental results indicate that the proposed method could achieve much higher accuracy and much greater consistency than LBIC, and it would thus benefit the defect recognition method greatly. The equivalent MSE gain of the proposed OMLBIC method reached a maximum of 16,384 for 128 × 128 test points without any additional scanning time or hardware upgrade requirements. Overall, the proposed modulation algorithm enhanced the noise immunity of the LBIC method greatly, and also resulted in significant improvements in both scanning accuracy and uniformity. The proposed method can be applied widely to perform detailed inspection, classification, and performance research for photovoltaic devices.

Declaration of Competing Interest

The authors declare that they have no known competing financial interests or personal relationships that could have appeared to influence the work reported in this paper.

Acknowledgement

We thank David MacDonald, MSc, from Liwen Bianji (Edanz) (www.liwenbianji.cn/) for editing the English text of a draft of this manuscript.

References

Acciarri, M., Binetti, S., Racz, A., Pizzini, S., Agostinelli, G., 2002. Fast LBIC in-line characterization for process quality control in the photovoltaic industry. Sol. Energy Mater. Sol. Cells 72 (1), 417–424.
Azim, M., 2013. Integration of the Output of A silicon Solar cell to the Grid System.
Bliss, M., Koutsourakis, G., Betts, T., Gottschalg, R., 2016. Development of a solar cell spectral response mapping system using multi-LBIC excitation.
Carstensen, J., Popkirov, G., Bahr, J., Föll, H.J.S.E.M., Cells, S., 2003. CELLO: an advanced LBIC measurement technique for solar cell local characterization. 76 (4), 599–611.
Chen, H., Pang, Y., Hu, Q., Liu, K., 2020. Solar cell surface defect inspection based on multispectral convolutional neural network. J. Intell. Manuf. 31 (2), 453–468.

Demirci, M.Y., Beşli, N., Gümüşçü, A., 2021. Efficient deep feature extraction and classification for identifying defective photovoltaic module cells in Electroluminescence images. Expert Syst. Appl. 175, 114810.
Fuyuki, T., Kitiyanan, A., 2009. Photographic diagnosis of crystalline silicon solar cells utilizing electroluminescence. Appl. Phys. A 96 (1), 189–196.
Fuyuki, T., Kondo, H., Yamazaki, T., Takahashi, Y., Uraoka, Y., 2005. Photographic surveying of minority carrier diffusion length in polycrystalline silicon solar cells by electroluminescence. Appl. Phys. Lett. 86 (26), 262108.
Geisthardt, R.M., Sites, J.R., 2014a. Light-beam-induced-current characterization of CdTe solar cells. In: 2014 IEEE 40th Photovoltaic Specialist Conference (PVSC), pp. 1848–1851.
Geisthardt, R.M., Sites, J.R., 2014b. Nonuniformity Characterization of CdTe Solar Cells Using LBIC. IEEE J. Photovoltaics 4 (4), 1114–1118.
Hall, S.R.G., Cashmore, M., Blackburn, J., Koutsourakis, G., Gottschalg, R., 2016. Compressive Current Response Mapping of Photovoltaic Devices Using MEMS Mirror Arrays. IEEE Trans. Instrum. Meas. 65 (8), 1945–1950.
Harwit, M., Sloane, N.J.A., 1979a. Appendix - Hadamard and S-Matrices, Walsh Functions, Pseudo-Random Sequences, and the Fast Hadamard Transform. Hadamard Transform Optics. Academic Press 200–228.
Harwit, M., Sloane, N.J.A., 1979b. Chapter 3 - The Basic Theory of Hadamard Transform Spectrometers and Imagers. In: Harwit, M., Sloane, N.J.A. (Eds.), Hadamard Transform Optics. Academic Press, pp. 44–95.
Jeco, B.M.Y., Sogabe, T., Ogura, A., Miyashita, N., Tamaki, R., Okada, Y., 2016. Laser beam induced current (LBIC) mapping of InGaP/GaAs/Ge triple junction solar cells with luminescence coupling, 2016 IEEE 43rd Photovoltaic Specialists Conference (PVSC). IEEE 1229–1234.
Kaminski, A., Breitenstein, O., Boyeaux, J.P., Rakotoniaina, P., Laugier, A., 2003. Light beam induced current and infrared thermography studies of multicrystalline silicon solar cells. J. Phys.: Condens. Matter 16 (2), S9–S18.
Kittler, M., Seifert, W., Arguirov, T., Tarasov, I., Ostapenko, S., 2002. Room-temperature luminescence and electron-beam-induced current (EBIC) recombination behaviour of crystal defects in multicrystalline silicon. Sol. Energy Mater. Sol. Cells 72 (1), 465–472.
Koktavy, P., Vanek, J., Chobola, Z., Kubickova, K., Kazelle, J., 2007. Solar cells noise diagnostic and LBIC comparison, AIP Conference Proceedings. American Institute of Physics 306–309.
Koutsourakis, G., Cashmore, M., Bliss, M., Hall, S.R.G., Betts, T.R., Gottschalg, R., 2016. Compressed sensing current mapping methods for PV characterisation. In: 2016 IEEE 43rd Photovoltaic Specialists Conference (PVSC), pp. 1308–1312.
Koutsourakis, G., Wu, X., Cashmore, M., Hall, S.R., Bliss, M., Betts, T., Gottschalg, R., 2015. Fast current mapping of photovoltaic devices using compressive sampling.
Kumar, P., Ghosekar, I., Narayan, K.S., 2021. High-Speed Laser Beam Induced Current Imaging: A Complementary Quantitative Diagnostic Tool for Modules. IEEE J. Photovoltaics 11 (6), 1436–1445.
Lim, J.C., Lorenzo, P.A.C., Macabebe, E.Q.B., 2015. Cost-effective LBIC system for solar cell characterization, TENCON 2015–2015 IEEE. Region 10 Conference, 1–4.
Motchenbacher, C.D., Connelly, J.A., 1993. Low-noise electronic system design. Wiley, New York.
Orlov, V.I., Feklisova, O.V., Yakimov, E.B., 2014. A comparison of EBIC, LBIC and XBIC methods as tools for multicrystalline Si characterization. Solid State Phenomena. Trans Tech Publ 142–147.
Podlaskin, B.J.T.P., 2007. Spatial filtering of temporal noise with the Hadamard transformation applied to a photodetector array. 52 (5), 672–675.
Pulfrey, D.L., 1978. MIS solar cells: A review. IEEE Trans. Electron Devices 25 (11), 1308–1317.
Quan, L., Xie, K., Liu, Y., Zhang, H., 2019. Camera enhanced compressive light beam induced current sensing for efficient defect detection in photovoltaic cells. Sol. Energy 183, 212–217.
Quan, L., Xie, K., Xi, R., Liu, Y., 2017. Compressive light beam induced current sensing for fast defect detection in photovoltaic cells. Sol. Energy 150, 345–352.
R2020b, M., 2020. Image Processing Toolbox for Use with MATLAB %J The MathWorks Inc.
Reuter, P., Rath, T., Fischereder, A., Trimmel, G., Hadley, P.J.S., 2011. Electron Beam-Induced Current (EBIC) in solution-processed solar cells. 33 (1), 1–6.
Sites, J.R., Nagle, T.J., 2005. LBIC analysis of thin-film polycrystalline solar cells. Conference Record of the Thirty-first IEEE Photovoltaic Specialists Conference 2005, 199–204.
Streeter, L., Burling-Claridge, G., Cree, M., Künnemeyer, R., 2009. Optical full Hadamard matrix multiplexing and noise effects. Appl. Opt. 48 (11), 2078–2085.
Su, B., Chen, H., Zhou, Z., 2022. BAF-Detector: An Efficient CNN-Based Detector for Photovoltaic Cell Defect Detection. IEEE Trans. Ind. Electron. 69 (3), 3161–3171.
Tripathi, J.N., Sharma, V.K., Shrimali, H., 2019. A Review on Power Supply Induced Jitter. IEEE Trans. Compon. Packag. Manuf. Technol. 9 (3), 511–524.
Vorasayan, P., Betts, T.R., Tiwari, A.N., Gottschalg, R., 2009. Multi-laser LBIC system for thin film PV module characterisation. Sol. Energy Mater. Sol. Cells 93 (6), 917–921.
Wang, Y., Li, L., Sun, Y., Xu, J., Jia, Y., Hong, J., Hu, X., Weng, G., Luo, X., Chen, S., Zhu, Z., Chu, J., Akiyama, H., 2021. Adaptive automatic solar cell defect detection and classification based on absolute electroluminescence imaging. Energy 229, 120606.
Zhao, Y., Yuan, S., Chang, Q., Zhou, Z., Kou, D., Zhou, W., Qi, Y., Wu, S., 2021. Controllable Formation of Ordered Vacancy Compound for High Efficiency Solution Processed Cu(In, Ga)Se2 Solar Cells. Adv. Funct. Mater. 31 (10), 2007928.